Chapter 3

$Ni_{25}Ti_{50}Cu_{25}$ Shape Memory Alloy Produced by Nonconventional Techniques

Tomasz Goryczka

Additional information is available at the end of the chapter

http://dx.doi.org/10.5772/48764

1. Introduction

Titanium-nickel alloys with a chemical composition close to equiatomic remain in the centre of interest due to the unique properties associated with shape memory effect (SME). In opposite to polymers or ceramic, mechanism of the shape memory effect is strictly correlated to the thermoelastic reversible martensitic transformation (MT). Modification of the course of the martensitic transformation influences the shape memory effect. Generally, course of the martensitic transformation can be influenced, separately or simultaneously, by two ways:

- Modification of chemical composition: addition and/or substitution of the alloying elements (Otsuka at all 1998; Van Humbeeck 1997). Alloying elements such as aluminum, iron, cobalt, cause lowering temperatures of the martensitic transformation even down to -140°C. Addition of copper (Duerig at all 1990), hafnium or zirconium (Li at all 2006) causes an increase of the transformation temperatures. In case of hafnium and zirconium, it is possible to obtain high-temperature shape memory alloys, in which the reversible martensitic transformation occurs at temperatures between 300 and 400°C (Santamarta at all 1999; Monastyrsky at all 2002).
- Modification of microstructure: way of production and/or farther alloy processing. The course of the martensitic transformation and its reversible nature is also affected by the structure of defects formed during the manufacturing or alloy processing. In order to change the transformation temperatures, in fact - the thermal range of the shape memory effect, mostly heat treatment or thermo-mechanical treatment is applied (Besseghini at all 1999; Kima at all 2006; Morawiec at all 1996). However, this requires an additional investments expenditure on devices. In consequence, it increases time of production process as well as its total cost.

Ternary NiTiCu alloy belongs to a large family of Ni-Ti alloys, which reveals shape memory effect (Mercier at all 1978). In the NiTiCu alloys content of titanium is close to 50at.% while

nickel does not exceed 20at.%. The rest is copper (Melton at all 1979). Substituting either nickel or titanium results in increasing the characteristic temperatures of the martensitic transformation, when compared to a binary NiTi alloy. In results of that, a thermal range of the shape memory effect moves from the room temperature up to approximately 80^0C (Duerig at all 1990). Moreover, copper causes good stability of transformation temperatures as well as prevents from formation of Ti_3Ni_4 precipitation (Fukuda at all 1995). However, the most important feature is appearance of the multistep martensitic transformation and formation of different type of the martensite structures. It results in receiving shape memory alloy, in which a hysteresis of the martensitic transformation can be narrowed from about 30 degrees down to 15 degrees. Dependently on the copper addition, the course of the martensitic transformation can be as follows (Nam at all 1990; Nomura at all 1990; Nomura at all 1992):

- the copper lower than 5-10 at% during cooling the parent phase B2 transforms directly to the B19' monoclinic martensite; thermal hysteresis is about 20 degrees;
- for 10-15at% Cu - transformation occurs in two steps: first, from the B2 parent phase the orthorhombic martensite B19 is formed, next the B19 martensite transforms to the B19' monoclinic martensite; thermal hysteresis is about 30 degrees;
- when the Cu content exceed 20%, again one-step transformation can be observed, however the B2 parent phase transforms directly to the B19 orthorhombic martensite; thermal hysteresis is about 10 degrees;

Special attention was drawn by alloy with nickel content of 25 at.% Ni and copper also 25 at.%. It was due to the wide possibility of its potential application (Gil at all 2004; Grossmann at all 2009; Colombo at all 2006) . The reason for this is the narrow thermal hysteresis loop of the martensitic transformation. Its width does not exceed 15^0C.

Recently, for manufacturing of the NiTi-based alloys, intensive effort has been put to adoption of the nonconventional production techniques such as powder metallurgy (PM) (Goryczka at all 2008); Li, 2000), melt-spinning (MS) (Santamarta at all 2004; Morgiel at all 2002; Goryczka at all 2001; Rosner at all 2001) or twin roll casting (TRC) (Goryczka and Ochin 2005; Dalle at all 2003; T. Goryczka, (2004)). This creates a wider possibility of the alloy applications. Despite the fact that these techniques have been successfully applied to metals and alloys production, their application for SMAs manufacturing is quite new.

The subtle nature of martensitic transformation and shape memory effect requires the selection of appropriate process conditions and parameters. In fact not many references about the influence of the processing parameters on the shape memory alloys and transformation behavior in NiTiCu alloy can be found.

The chapter is focused on $Ni_{25}Ti_{50}Cu_{25}$ alloy manufactured by powder metallurgy or rapid solidification techniques. Comparison of transformation behavior, structure, and microstructure is discussed.

2. Powder metallurgy

2.1. From powders to alloy

In order to produce NiTiCu alloy with the nominal chemical composition (25at.% Ni, 50at.% Ti and 5at.% Cu) commercial powders of elements (purity 99,7%) were weighted in proper ratio and mixed in a rotary mixer during 48 hours. Measured average particle size of as-received powders was 6.2 μm, 11.5 μm and 33.7 μm for Cu, Ni and Ti, respectively (Fig. 1).

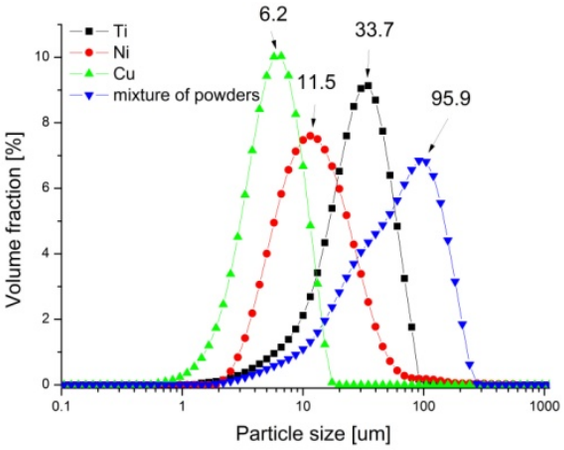

Figure 1. Particle size distribution for powders and their mixture.

During mixing the mixture was homogenized. Simultaneously, powders were agglomerated in mechanical alloying process (Fig. 2a). Due to the significant differences in hardness of the alloying elements (Cu - 369HV, Ti - 970HV, Ni - 638HV), this effect becomes clear between Ti and Cu as well as Ni and Cu. Figure 2b shows distribution of the elements from region marked in Figure 2a . The large particles were composed of Cu and Ti powders as well as Cu and Ni. In consequence, the powders were homogenously distributed in the mixture and its average particle size increased up to 95.9 μm (Fig. 1).

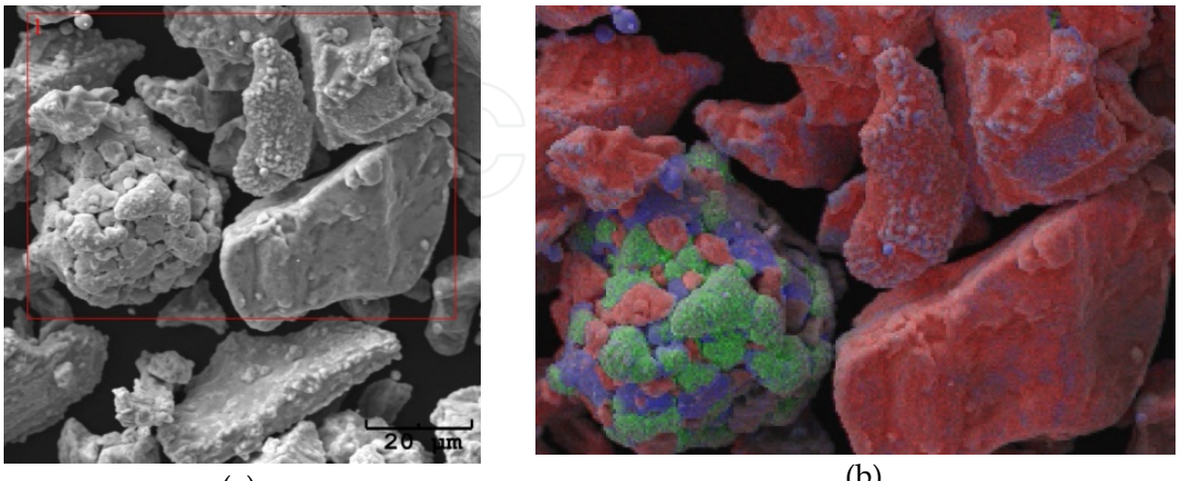

(a) (b)

Figure 2. SEM image of the powder's mixture (a) and distribution of the elements from region marked in left image (red – titanium, green - nickel, blue – copper) (b).

From mixture, compacts were formed at room temperature under pressure of 8 MPa. They were in a shape of cylinder with diameter of 10 mm and 6 mm high. Sintering was carried out in a horizontal tube furnace under argon atmosphere. Sintering conditions were chosen in reference to the melting temperature (1264^{0}C). It varied from 850^{0}C to 1100^{0}C and total sintering time from 7 to 20 hours. After sintering, furnace was slowly cooled down to the room temperature.

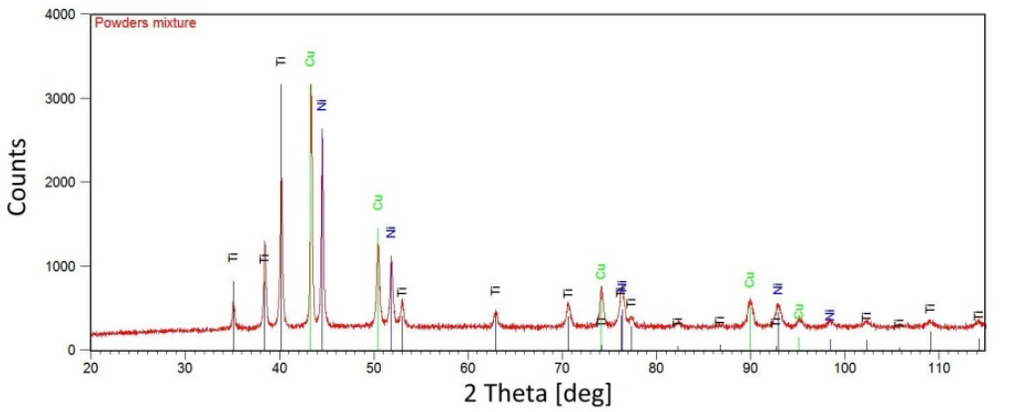

(a)

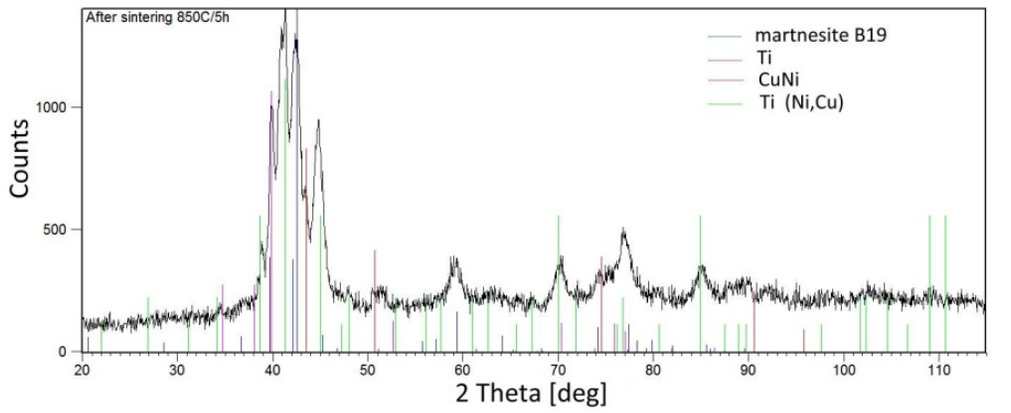

(b)

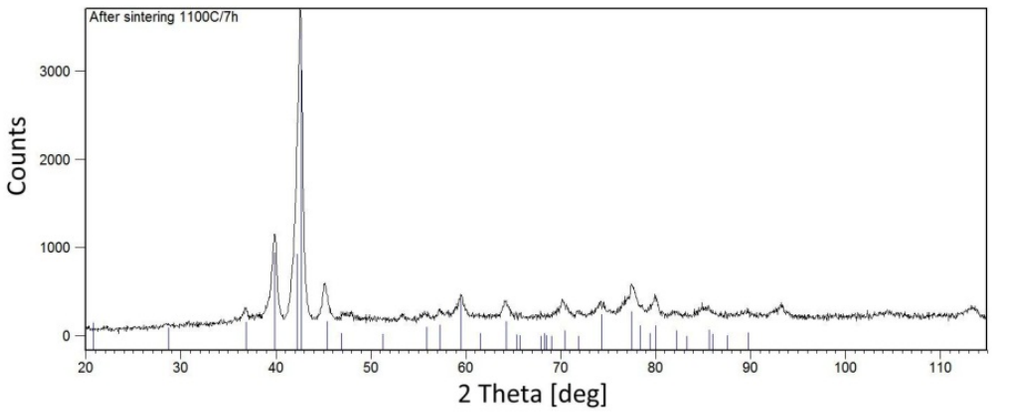

(c)

Figure 3. X-ray diffraction patterns registered for powders mixture (a), alloy sintered at 850^{0}C for 5 hours (b) and at 1100^{0}C for 7 hours (c).

In order to prove, that after sintering the NiTiCu alloys were obtained, X-ray diffraction analysis was done for compacts as well as blends. X-ray diffraction pattern were measured using the X'Pert Pro diffractometer with Cu radiation ($K_{\alpha 1 \text{ and } \alpha 2}$) in the 2θ range: 20 ÷ 140 degrees. Figure 3a shows X-ray diffraction pattern registered for compact before sintering. It can be clearly seen that diffraction pattern contains diffraction lines, which belongs to the pure alloying elements. Separated phases were identified using the ICDD data base PDF-2. It was proved that powders mixture consisted from Ti, Ni and Cu (card no Ti: 065-3362; card no Ni: 04-0850 and card no Cu: 04-0836). Moreover, quantitative analysis done using the Rietveld refinement confirmed that measured chemical composition was comparable to the nominal one. The main goal of sintering was to produce transformable phase, which can be described by nominal chemical composition of the alloy as $Ni_{25}Ti_{50}Cu_{25}$. For such composition, in a bulk alloy, the orthorhombic B19 martensite appears. It undergoes martensitic transformation at temperature above 75^0C creating the B2 parent phase (Duerig at all 1990). X-ray diffraction patterns registered at room temperature showed that independently on applied sintering conditions, the orthorhombic B19 martensite was found in all blends. However, sintering took an effect on the phase composition. One has to remember that mechanism of the alloying, which occurs during sintering is different from that, in tradition melting. During sintering alloying elements diffuse each one into other. Thus, from the ternary powder mixture reaction between alloying elements may be combined. In result of that various phases coming from the systems: Ni-Ti, Cu-Ni as well as Cu-Ti may be expected (Gupta 2002). Precursor of that is partial mechanical alloying, which occurred during powders mixing (Fig. 2).

Sintering conditions		Fraction of phase [%]			
Temperature [^{0}C]	Time [h]	B19	Ti_2(Ni,Cu)	NiCu	Ti
850	5	82.7 ± 2.9	13.7 ± 0.6	2.4 ± 0.3	1.2 ± 0.2
	10	83.9 ± 3.7	16.1 ± 0.6	-	-
	20	86.1 ± 2.9	13.9 ± 0.5	-	-
950	7	89.7 ± 1.9	10.3 ± 0.3	-	-
1100	7	100	-	-	-

Table 1. Results of quantitative phase analysis done for blends sintered at various conditions

Lower sintering temperature in combination with short sintering time was not enough to provide a support for diffusion of the alloying elements. In consequence, apart of the B19 martensite also equilibrium phases appeared in sintered blends. Figure 3b shows X-ray diffraction pattern measured, at room temperature, for the blend sintered at 850^0C for 5 hours. Qualitative phase analysis revealed that the blend contained also phases such as: NiCu (PDF-2 card no 47-1406), Ti_2(Ni,Cu) – which has crystallographic structure of the Ti_2Ni phase (PDF-2 card no 05-0687) as well as a solid solution of Ni in Ti (PDF-2 card no 89-3073). In order to study of phase contribution in sintered blends the Rietveld refinement was done. Values of reliability factors, which prove goodness of the refinement, were below 8%. Obtained results were compared in Table 1. Quantitative analysis showed that amount of the B19 martensite was about 83% in blends sintered at 850^0C for 5 hours. Extending of the

sintering time up to 10 hours was enough for nickel and cooper diffusion. Both phases: NiCu and pure titanium were not observed. Extending of the sintering temperature resulted in the limitation of the $Ti_2(Ni,Cu)$ phase formation. The best sintering condition was: temperature 1100^0C with sintering time of 7 hours. In the sintered blend only the B19 martensite was identified (Fig. 3c).

Obtained results were confirmed by observation carried out using the JEOL JSM 6480 electron scanning microscope. Observations were done on a circular cross-section of the cylindrical blends. Figure 4 shows images taken using back scattered electrons. In places, which varied in a contrast, a chemical composition was determined using energy-dispersive X-ray analysis (EDX) in the JEOL JSM 6480 microscope. Measurements were done in macro scale and 50 points were taken for calculation. Calculated ratio of the alloying elements was in a good correlation with the phases identified with use of X-ray diffraction analysis. SEM image observed for the blends, sintered at 1100^0C for 7 hours, proved that only the B19 martensite was present at the sample (Fig. 4a).

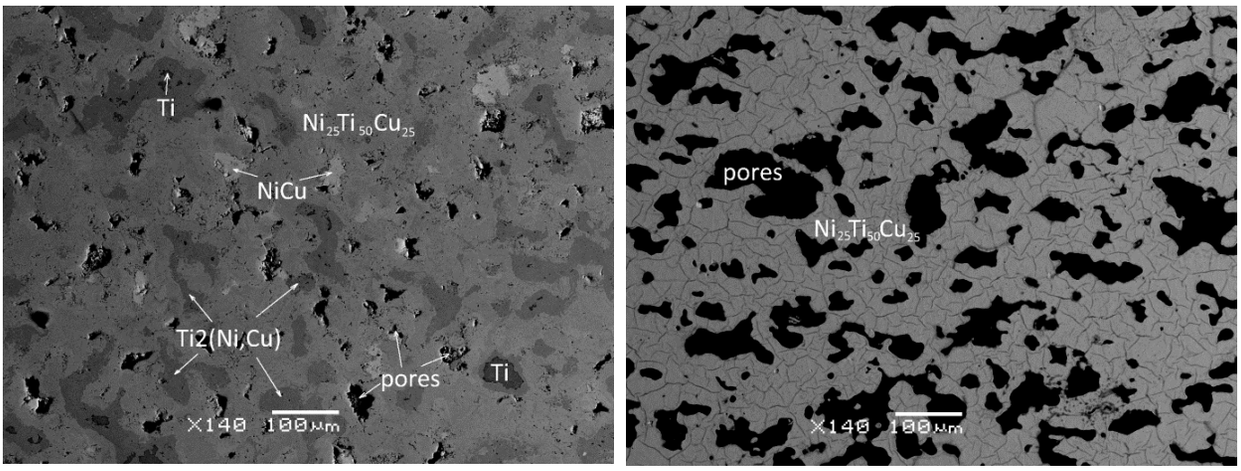

(a) (b)

Figure 4. SEM images observed at a cross-section of blends sintered at 850^0C for 5 hours (a) and 1100^0C for 7 hours (b)

Sintering, mainly used for ceramic production, also produces pores. Their amount, size and distribution strictly depend on sintering condition as well as particle size of the elemental powders. Dependently on final application of the product, presence of the pores can be considered as a desired element of the microstructure. For example, in medical application pores can be considered as wanted ones, in which the collagen fiber finds way to grow-in. However, their diameter has to be appropriate and varied from 50 to 500 μm (Karageorgiou 2005; Itala 2001; Simske 1995). In case of shape memory alloys, pores do not provide a material, which undergoes the martensitic transformation. For that reason they can be considered as not desired element of the microstructure. In comparison to a bulk material, from the same volume of the sintered alloy lower transformation enthalpy can be received (Yuan 2006). Also, pores form natural barrier for diffusion of alloying elements. It may lead to inhomogeneity even in the frame of grains of the same phase. In order to overcome such

inconvenience, sintering time should be extended and/or higher sintering temperature is required.

To bring more light for this problem in the $Ni_{25}Ti_{50}Cu_{25}$ alloy, amount of pores was calculated basing on the SEM images taken over whole cross-section of the sample.

In general, the porosity in alloy sintered at 850^0C did not exceed 5% (Fig. 5a). The pores were randomly distributed and clearly separated (Fig. 4a). However, pore size varied dependently on the sintering time. The average pore size in the alloy sintered 5 hours was about 8 μm (Fig. 5a). Increase of the sintering time to 20 hours was responsible for increase of the pore size to 38 μm. It is worthy to notice, that calculated values of standard deviation for pore size, in the alloys sintered for 5 or 10 hours, are very close (Fig. 5a). It means that relatively short sintering time did not influence on scattering of the pores size. The pores have similar diameter and were comparable in a shape. Completely different value of standard deviation was obtained for the alloy sintered for 20 hours. It was ±15 μm. Extending of the sintering time up to 20 hours caused formation of the pores, which varied in size from about 8 μm up to 60 μm. In most cases they have irregular shape.

Significant differences in porosity, size of pores and pores distribution can be observed for samples, which were produced applying higher temperatures (Fig. 4b). Increase of the sintering temperature up to 950^0C or 1100^0C caused increase of porosity up to 21% or 27%, respectively (Fig. 5). However, alloy sintered at 950^0C revealed comparable morphology to one observed in alloy sintered at 850^0C for 5 or 10 hours. The pores, with average diameter of 41 μm, possessed similar regular elliptical shape. Increase of the sintering temperature up to 1100^0C caused differences in shape and distribution of pores. Average diameter of pores increased to 50 μm. Higher value of the standard deviation indicated that they varied in shape and size. At 1100^0C diffusion of alloying elements was more intense. In result of that, most of the small pores were joined into large one forming their irregular shape (Fig. 4b).

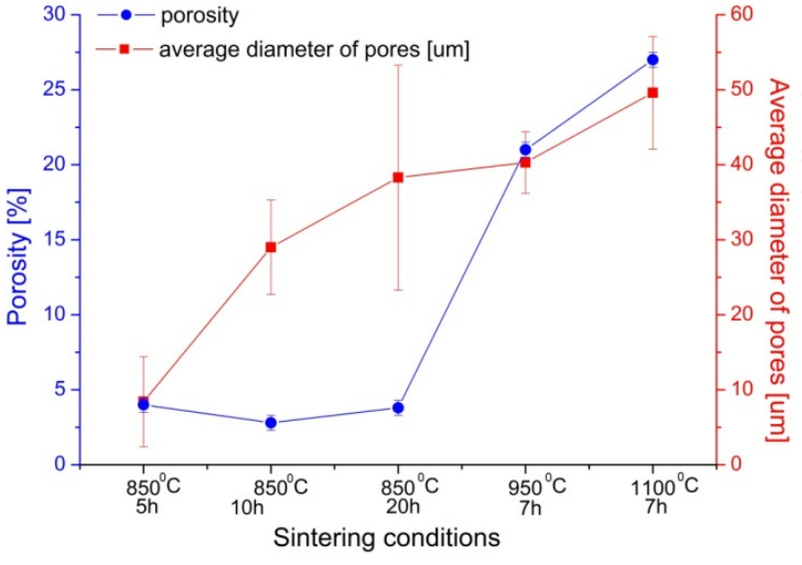

Figure 5. Porosity and average diameter of pores versus sintering conditions

2.2. Martensitic transformation

In order to show influence of the sintering condition on the course of the martensitic transformation DSC cooling/heating curves were registered at temperature range between -100^{0}C and +200^{0}C. Measurements were done using differential scanning calorimeter Perkin Elmer DSC-7 with cooling/heating rate of 10^{0}C /min. Evolution of the DSC cooling/heating curves registered for sintered alloys is shown in Figure 6a. The characteristic temperatures of the martensitic transformation (start M_s, A_s and finish M_f, A_f of the forward and reveres transformation, respectively) were determined using a slope line extension method. Enthalpy of transformation was calculated from the thermal peak (Fig. 6b).

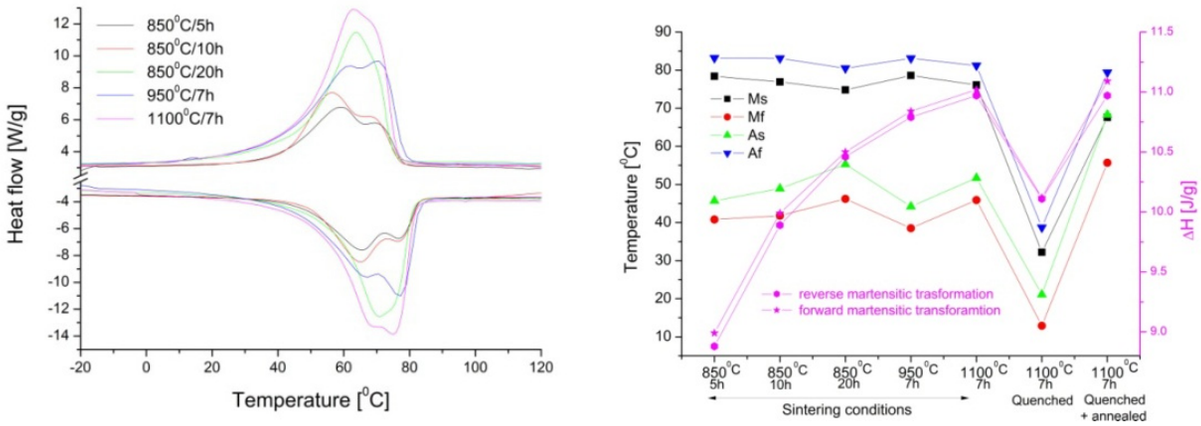

(a) (b)

Figure 6. DSC cooling/heating curves (a) and parameters of the martensitic transformation (b) for alloy sintered at various conditions

Generally, all sintered alloys reveal presence of the reversible martensitic transformation. Thus, the main condition for appearing of shape memory effect is satisfied. However, course of the martensitic transformation varies dependently on applied sintering conditions. First, the M_s and A_f temperatures show general tendency for decreasing when the condition for diffusion of alloying elements improves. In opposition to that, the A_s and M_f increases. It takes an effect on thermal ranges of the transformation. Second, the martensitic transformation occurs as one step or two steps transition.

Let's discuss firstly change of the chemical composition as a result of the presence of non-transformable the Ti_2(Ni,Cu) phase. It posses the same type of the crystal structure as the Ti_2Ni phase. In the Ti_2(Ni,Cu) phase, the ratio of Ni atoms to Cu is as 30:1. The presence of this phase decreases titanium content in the transformable phase. Also, one have to keep on mind that the fraction of the Ti_2(Ni,Cu) phase decreases from 16% to 0% dependently on sintering conditions. In consequence, the M_s temperature slightly moved to lower region. Influence of the chemical composition on the M_s temperature has been known and used as key feature in designing of shape memory alloy. However, in ternary alloys this problem is more complex. The thermal behavior of the NiTiCu alloy depends on titanium-nickel ratio as well as nickel-copper ratio. Hanlon et all (Hanlon 1967) shown, that in the NiTi alloy with

titanium content around 50-51at% takes a little effect on the M_s temperature. However, when the titanium content lowers from 50 to 49at% the M_s temperature may decrease from 50^0C to -140^0C, respectively. In opposition to that increase of copper content, instead of nickel atoms, causes increase of the M_s temperature. For the B2↔B19 transformation in NiTiCu bulk, Mobelry and Melton (Moberly and Melton 1990) showed that increase of copper content from 20 to 25 at% caused increase of the M_s from 48^0C to 76^0C, respectively.

The presence of the non-transformable phase takes an effect on the transformation enthalpy (Fig. 6b). Enthalpy of the transformation, at fully transformable bulk alloy, equals about 12 J/g (Hanlon 1967). Presence of non-transformable phases decreases an amount of the phase, which undergoes the martensitic transformation. In result of that, the transformation enthalpy decreases.

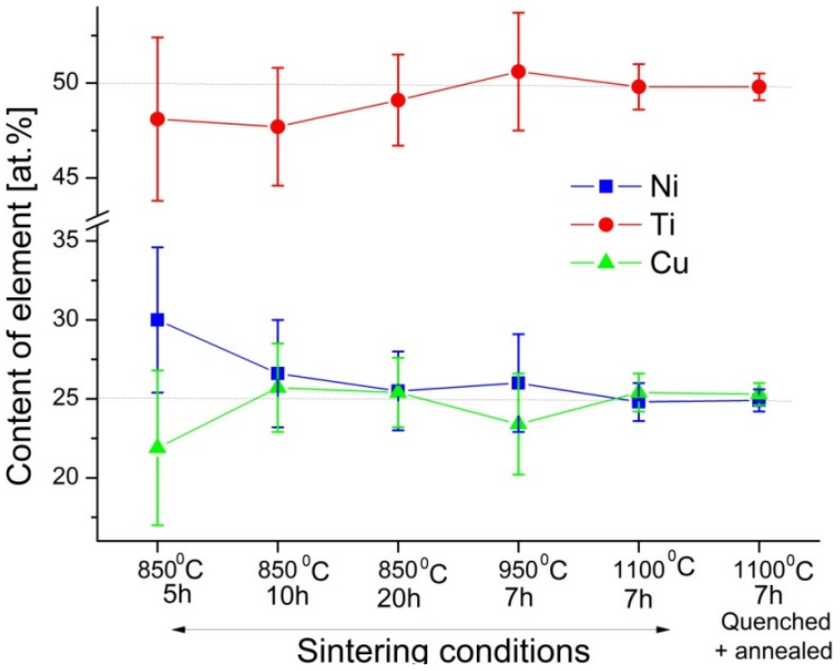

Figure 7. Distribution of the alloying elements, in the transformable phase, versus sintering conditions

The thermal behavior of the sintered alloy may also be a consequence of inhomogeneity of the chemical composition inside of the transformable phase. Figure 7 shows the distribution of the elements versus sintering conditions. Measurements were done in the transformable phase. Calculation of the chemical composition was done over 50 points spread on the cross-section of the sample. It has been clearly seen that a distribution of alloying elements, close to the nominal composition, was obtained in blends sintered at 1100^0C for 7 hours. It was as follows: Ti - 49.8at.%, Ni - 24.8 at.% and Cu-25.4 at.%. In order to analyze the homogeneity or inhomogeneity, a standard deviation was marked as a vertical bar. The sintering at 1100^0C for 7 hours causes a small deviation from the average content of the alloying elements and is characterized by relatively low value of the standard deviation. The value of the standard deviation calculated for sintering temperature 850^0C and time 5 hours or 10 significantly increases to 5% for Ni and Cu as well as for Ti up to 4%. High inhomogeneity

of these samples eliminates them as a shape memory material. Lower values of the standard deviation (about 3%) were obtained for sintering at 950^{0}C and 10 hours. However, in this alloy Ti content increased up to 50.6at.%. This was a reason for increase of the M_s temperatures to 78.6^{0}C. In the sample sintered at 850^{0}C for 20 hours the standard deviation was about 2%. However, measured chemical composition slightly varied from the nominal one.

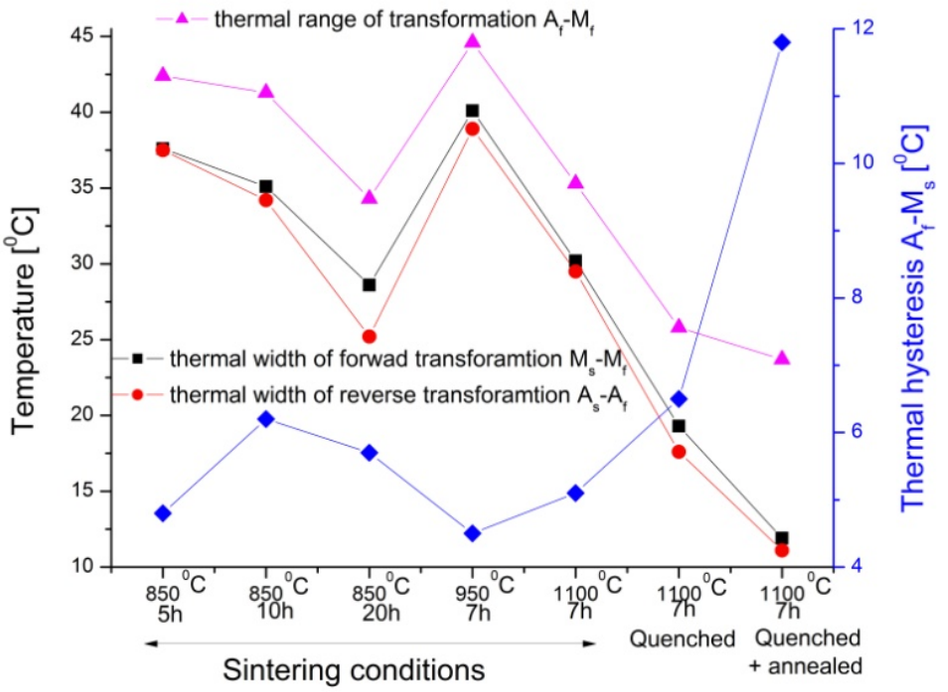

Figure 8. Thermal ranges of the reversible martensitic transformation versus sintering conditions

The local changes of the chemical and its inhomogeneity took an effect on the course of the martensitic transformation. For alloy, sintered at 850^{0}C for 5 hours, the DSC curves reveal two maxima on cooling (at 58.6^{0}C and 69.4^{0}C) as well as two minima on heating (at 65.4^{0}C and 76.8^{0}C). The range of the martensitic transformation (A_f–M_f) equals 42 degrees (Fig. 8 – green line). Thermal hysteresis (A_f–M_s) is about 5 degrees (Fig. 8 – blue line). Difference calculated between position of maximum (on cooling) and corresponding minimum (on heating) keeps comparable value (8^0). The range of the thermal peak on cooling (M_s-M_f) as well as heating (A_s-A_f) is wide and equaled 38^0 (Fig. 8 – red and black line, respectively). Measured X-ray diffraction pattern confirmed that at room temperature the B19 marteniste existed. Taking, all these facts into consideration, it can be concluded that the parent phase transforms to the B19 orthorhombic marteniste. However, in the thermal region of transformation two thermal peaks were overlapped. For such thermal behavior, inhomogeneity of chemical composition may be responsible. Calculated value of the standard deviation (Fig. 7) of measured composition shows significant inhomogeneity in samples. Regions of transformable phase, which differ in chemical composition, undergo martensitic transformation at close temperature, that's why two overlapped peaks were observed.

Neither elongation of the sintering time up to 10 hours nor rising sintering temperature up to 950^{0}C did not change course of the transformation – still two overlapped B2↔B19 transformations were observed. A completely different thermal behavior is observed in the alloys sintered at 850^{0}C for 20 hours as well as 1100^{0}C and 7 hours. Instead of two peaks, one peak was found on cooling as well as on heating. In case of both sintering conditions the range of the martensitic transformation (A_f–M_f) reduces to 34^0 (Fig. 8 – green line). Also, range of the thermal peak on cooling (M_s-M_f) as well as heating (A_s-A_f) narrows and equals 30^0 (Fig. 8 – red and black line, respectively). Thermal hysteresis (*Af*–*Ms*) slightly differs and for 850^{0}C/20 hours is about 5.7^0 and for 1100^{0}C/7 hours is lower and equals 5.1^0.

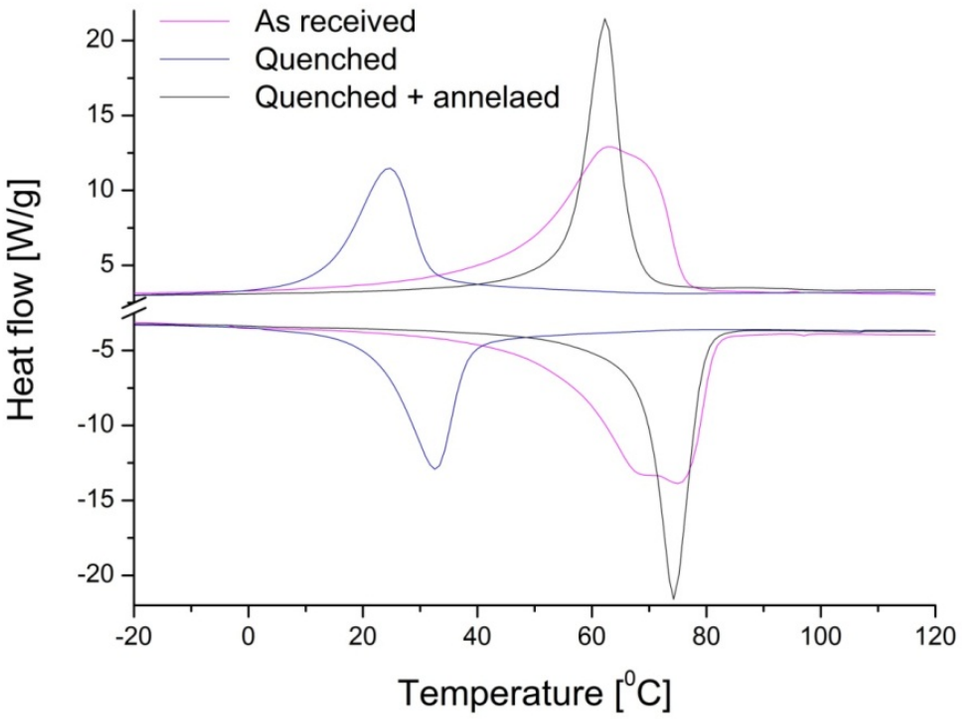

Figure 9. Comparison of DSC cooling/heating curves registered for alloy sintered at 1100^{0}C for 7 hours after additional thermal treatment

For both sintered blends irregular shape of the thermal peaks measured on DSC cooling/heating curves was stated. It also may results in slight differences in chemical composition of the transformable phase (standard deviation was 2.2% or 1.2%). In order to improve quality of the alloy sintered at 1100^{0}C/7 hours it was quenched from 900^{0}C and additionally annealed at 500^{0}C for 24 hours. Influence of thermal treatment on a course of the martensitic transformation is shown in Figure 9. First, only one thermal peak was measured during cooling as well as heating. It has symmetrical shape. Second, in comparison to the as-received sample, quenching moved down transformation temperatures of about 34 degrees (Fig. 6b). It is a result of quenched-in structural defects. This effect is better visible in rapidly solidified alloy and will be discussed in next subchapter. Additional annealing at 500^{0}C for 24 hours restored thermal region of the reversible martensitic transformation. In consequence, the M_s transformation temperature

was comparable to that calculated for the as-received sample (Fig. 8a). Summarizing, additional thermal treatment:

- did not change the chemical composition of the transformable phase: (Ti - 49.8at.%, Ni - 24.9 at.% and Cu-25.3 at.%);
- alloy was stable and did not decompose to equilibrium phases;
- homogeneity of the alloy was improved - calculated standard deviation of the chemical composition was 0.7%;
- the transformation enthalpy is comparable to that determined for bulk alloy (Fig. 6b) .

In result of that, the thermal range of the transformation as well as thermal width of forward and reversible transformation reduced to 23 degrees and 11 degrees, respectively (Fig. 8). However, width of the thermal hysteresis of the transformation increased from 6 (as-received sample) to 12 degrees. It may be caused by remains of the no-annealed point defects. Extending of the annealing temperature to 48 hours caused decomposition of the transformable phase. Again the $Ti_2(Ni,Cu)$ phase appeared.

3. Rapid solidification

Technologies for producing alloys in a finite shape directly from the molten state received a lot of attention. The rapid solidification techniques, realized in melt-spinning or twin roll casting technique, applied to the shape memory alloys offer not only a convenient and economical production technology but also possibilities to improve the alloys' properties as well as to control in a relatively easy way the temperatures of the reversible martensitic transformation. The increase in the wheel speed causes the grain refinement and changes their morphology from equiaxial to columnar (Eucken 1990; Stoobs 1979; Morawiec 2003).

3.1. Melt-spinning

In order to produce melt-spun ribbons, ingots with nominal chemical composition were cast in an induction furnace. Ingots weighted about 10 g. Casting was carried out in a pre-evacuated chamber before melting. Melt was ejected with pressure of 0.02 MPa on a rotating wheel. Increase of cooling rate was realized by increase of wheel speed and/or temperature of melt. Four ribbons were produced with processing parameters shown in Table 2.

Symbol	Melt temp. [^{0}C]	Wheel speed [m·s^{-1}]	Thickness [μm]	Width [mm]
MS1	1250	11	83	6,3
MS2	1250	15	64	5,9
MS3	1250	19	48	2,7
MS4	1350	23	46	5,2

Table 2. Processing parameters and dimension of the ribbons

Generally, high cooling rate in the melt–spinning technique (10^6 K/s) causes inhomogeneity of the microstructure on the surface of the ribbons. It is due to fact that the liquid alloy is ejected onto fast rotating wheel. Firstly, the side, which has directly contact with rotating wheel, undergoes solidification. Secondly, until crystallization goes thorough the ribbon, the cooling rate lowers, and finally, the top surface solidify. This procedure produces two different surfaces: one what could be called "frozen" metal from the contact side and second one – top surface.

The combination of the wheel speed (11 m/s) and temperature of melt (1250°C) provided the lowest rate of cooling. It results in elongation of the time, when the liquid alloy contacts surface of rotating wheel. It provides enough time for crystallization of columnar grains, which extends along thickness of the ribbon (Fig. 10a).

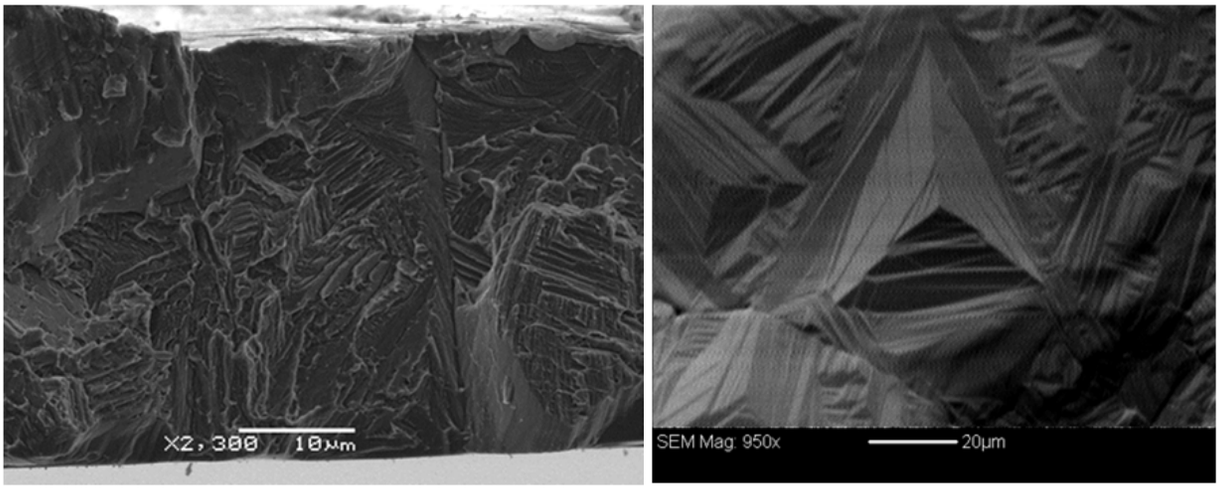

(a) (b)

Figure 10. SEM images observed at the fracture (a) and on the surface (b) of the ribbons MS2

On the surface of the MS1 ribbon self- accommodating plates of the martensite were observed (Fig. 10b). Similar images were observed in the MS2 ribbon, which was produced with higher wheel speed - 15 m/s. X-ray studies confirmed the presence of the B19 martensite. X-ray diffraction patterns registered at room temperature for the MS1 was identified as belonging to the B19 structure (Fig. 11 – "Ribbon MS1"). In case of the MS2 ribbon, apart from the B19 phase, the B2 parent phase was also identified (Fig. 11 – "Ribbon MS2"). It is a result of increase of the cooling rate, which caused increased of the structural defects quenched-in.

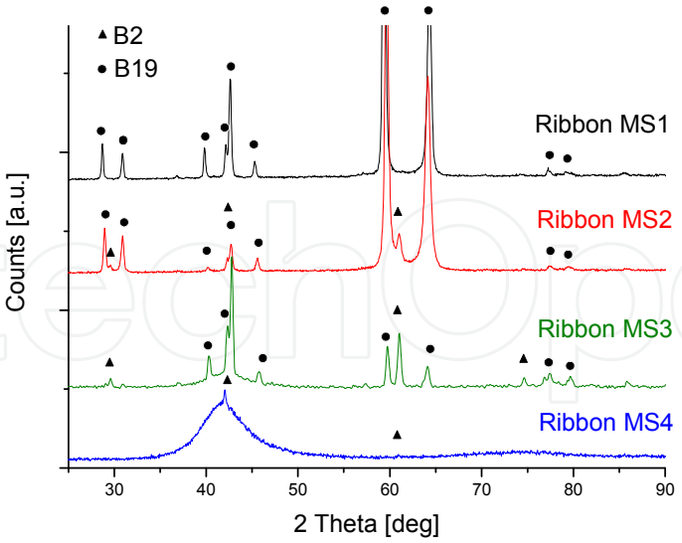

Figure 11. The X-ray diffraction patterns registered at room temperature for melt-spun ribbons

A different microstructure was observed in the MS3 ribbon (Fig. 12). Increase of the wheel speed to 19m/s, while the temperature of melt was the same (1250^{o}C), did not provide a sufficiently time for crystallization of columnar grains. At the thickness of the ribbon three zones were formed (Fig. 12a). First, an amorphous layer, 3-5 μm thick, was formed as a contact side of the ribbon. The second zone, formed during solidification, is the area consisted of spherical grains with an average diameter of about 5-8 micrometers. Finally, the zone composed of the columnar grain is formed, which extends to the top surface of the ribbon. Microstructure of the ribbon is inhomogeneous. Images observed at the fracture, taken from various part of the ribbon, show the columnar grains with width to 35 μm extended along whole thickness of the ribbon. At this area, no amorphous phase was observed. Also in some parts of the ribbon, only small spherical grains were formed along the thickness (Fig. 12b).

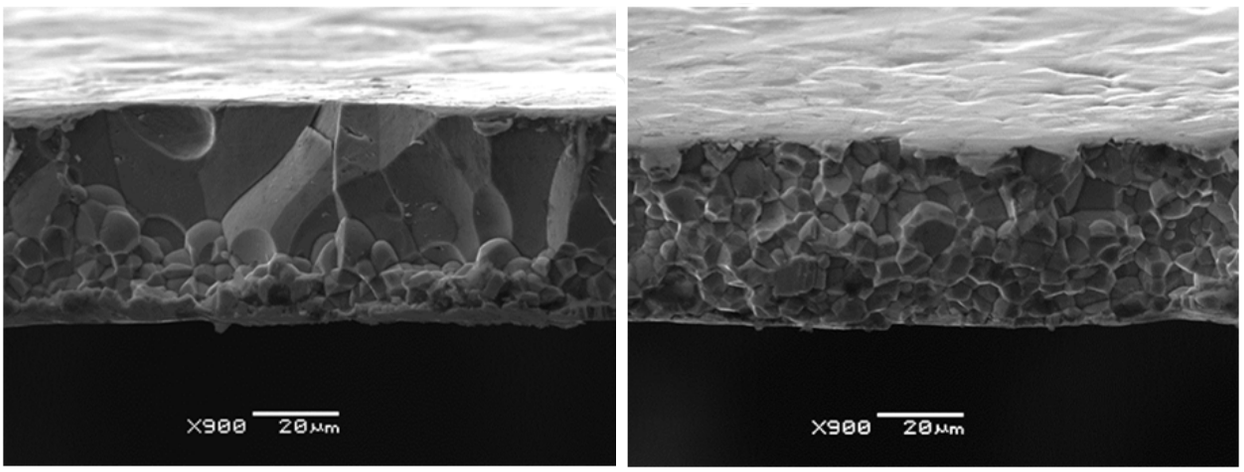

(a) (b)

Figure 12. SEM images observed at the fracture of the MS3 ribbon

Observation of the contact surface shows that this area is not homogeneous. Among the amorphous phase two groups of crystalline "islands" were observed (Fig. 13a). They were randomly distributed and differed in size. Diameter of the "islands" varied from 5 μm to 25 μm. Inside of crystalline areas the martensitic plates were clearly visible. The plates transforms to the parent phase after heating above A_f. After cooling, they reversibly transforms to the martensite.

X-ray diffraction patterns revealed that the MS3 ribbon consists of three phases: amorphous (weak broaden line), the B2 and the B19 (Fig. 11 – "Ribbon MS3"). Increase of the melt temperature to 1350^0C and wheel speed to 23 m/s formed almost amorphous ribbon - MS4. The cooling rate realized with these processing parameters does not provide enough time for full crystallization during solidification. The contact surface is completely amorphous. However, at the top surface some crystallized grain can be distinguished (Fig. 13b). The X-ray diffraction patterns shows two broaden maxima characteristic for the amorphous phase. Moreover, weak diffraction lines belonging to the B2 parent phase were identified (Fig. 11 – "Ribbon MS4").

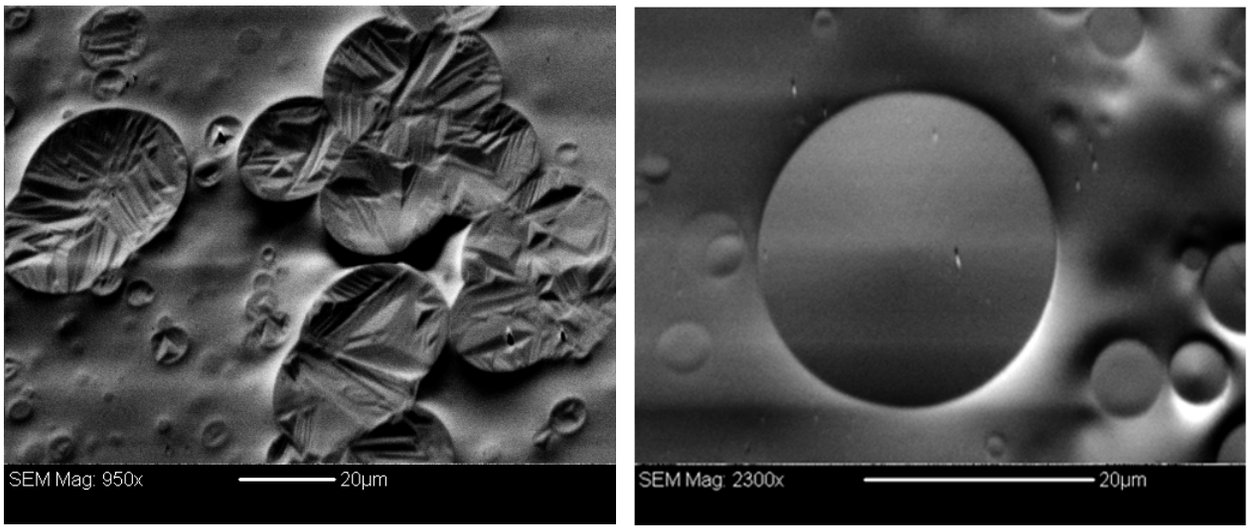

(a) (b)

Figure 13. SEM image of the contact side of the MS3 ribbons (a) and top surface of the MS4 ribbon (b).

From the point of the shape memory effect and the martensitic transformation presence of the amorphous phase is not desirable. The martensitic transformation as a coordinated atom movement at distance proportional to distance to the habit plane occurs only in the crystalline state. Presence of the amorphous phase increases amount of the transformable phase in the ribbons. In order to eliminate influence of the amorphous phase and quenched-in defects on the course of the martensitic transformation crystallization was carried out. Ribbon was heated up to 600^oC, and then cooled to 0^oC. Heating and cooling was done, inside of DSC calorimeter, with rate of 10 °C/min at argon atmosphere. Observed high temperature peaks correspond to the crystallisation process (Fig. 14). Crystallization of the amorphous phase starts at 445^oC and finishes at 466^oC. The value of enthalpy was 6.5 J/g. For further studies, the MS4 ribbon was used in crystalline state and denoted as "MS4C".

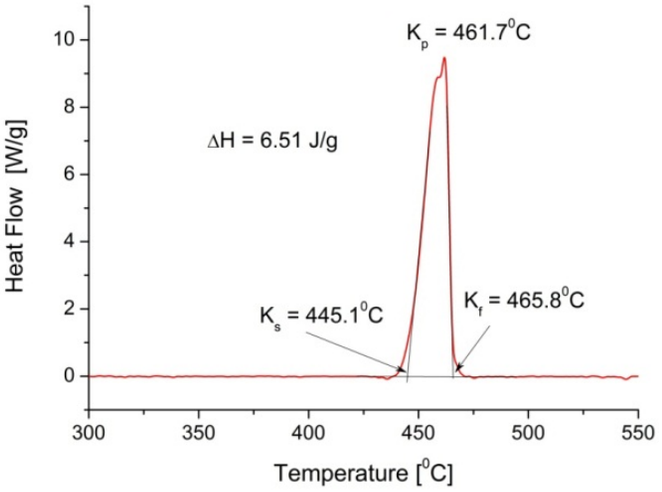

Figure 14. DSC heating curve registered for the MS4 ribbon

Applied casting parameters significantly influenced the course of the martensitic transformation. Figure 15a shows comparison of the DSC cooling/heating curves registered for the first cycle of heating-cooling. In order to obtain the full thermal cycle, the samples were cooled down to 0°C, then heated up to 110°C and again cooled to 0°C. The order and the shape of the thermal peaks occurring at thermograms proved that the martensitic transformation is reversible in all ribbons. However, they differ in the transformation temperatures. The DSC curves measured for the MS1 and MS4C ribbons contain one thermal peak on both heating and cooling curve, respectively. In comparison to that, the DSC curves measured for ribbons: MS2 and MS3 revealed a different course. The thermal peaks measured for the MS2 ribbon show irregular shape, whereas for the MS3 ribbon they were broadened and split. In result of that, for the MS3 ribbon two maxima at temperatures 33°C and 49°C for the forward martensitic transformation as well as two minima for the reverse transformation at 42°C and 55°C were found.

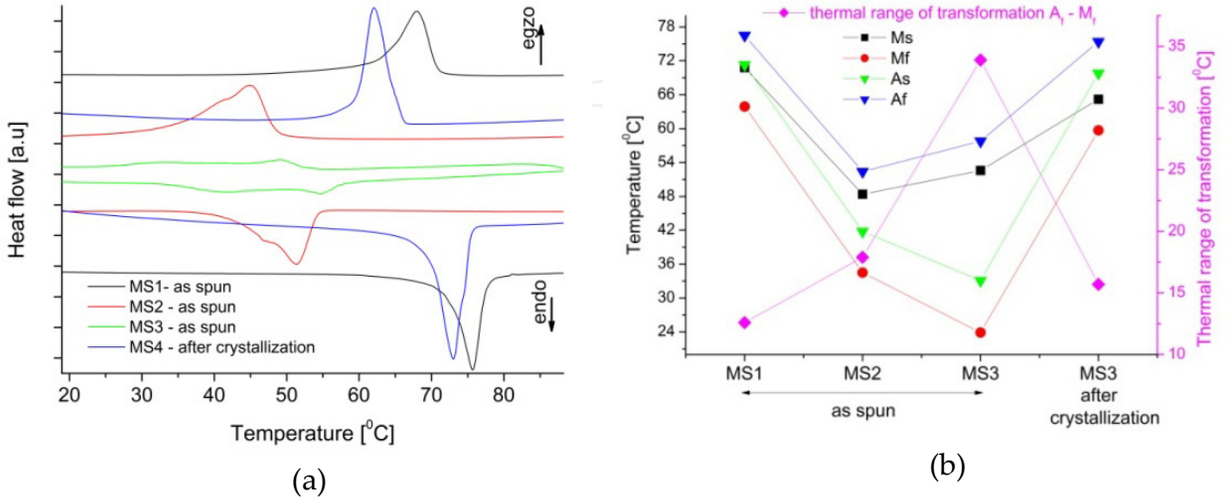

Figure 15. DSC cooling/heating curves measured for the melt-spun ribbons (a) and parameters of the martensitic transformation (b)

The combination of the wheel speed and the temperature of melt, applied in the case of the casting the MS1 ribbon ensured the lowest speed of solidification - similar to the equilibrium condition. The transformation temperatures, determined from DSC curves, are comparable to that determined for the MS4C ribbon (Fig. 15b). For alloys with low concentration of structural defects, the thermal range does not exceed 15 degrees. In the case of the MS1 and MS4C ribbon the thermal range of the martensitic transformation was 12 and 15°C, respectively.

Increase of the wheel speed to 15 m/s caused increase of the cooling rate in the MS2 ribbon. The density of the structural defects increased. Figure 16 shows an example of the image observed with use of the electron transition microscope. Relatively high density of dislocations can be distinguished. Dislocations as well as point defects increase local stress, which has to be overcome when the marteniste plates are formed. It requires additional overcooling and in consequence, the transformation temperatures moves to lower thermal region. In case of the MS2 ribbon transformation temperatures were lower of about 20 degrees in comparison that in the MS1 ribbon. Thermal range of the martensitic transformation increased to 18°C.

Further increase of the wheel speed to 19m/s caused increase of density of the structural defects. In comparison to the MS2 ribbon, the M_f and A_s temperatures decreased of about 8°C whereas the A_f and M_s increased of about 5°C. The thermal range of the martensitic transformation increased to 34°C.

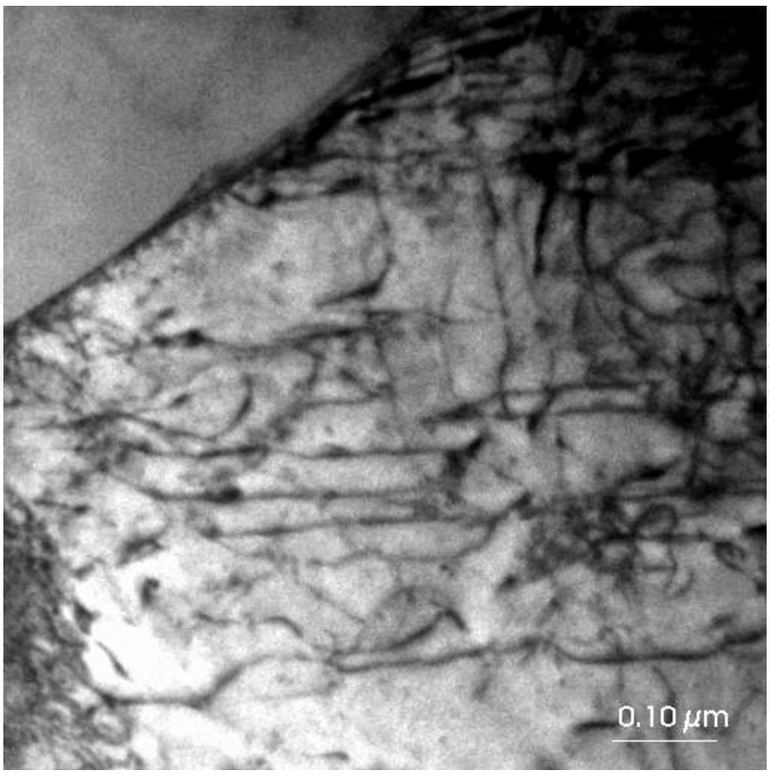

Figure 16. TEM image of the dislocation structure in the MS2 ribbon

3.2. Twin roll casting

Twin roll casting technique (TRC) has been known for almost 30 years in aluminum and iron casting industry (Berg, at all 1995) (Haga 2003). Thin strip, from 10 mm up to 0.5 mm, can be continuously produced replacing conventional processing techniques, which use an ingot and additional thermo-mechanical treatment (Goryczka, at all 2005). The main advantage of TRC is a relatively short processing route which joins casting as well as hot rolling in one step (Haga 2001). Also, low cost equipment, low energy consumption, space saving, strips are free of impurities which come from a crucible and surroundings etc. belong to the most desirable features of TRC technique. In spite of that, also, twin roll casting has some disadvantages. The main one is poorer mechanical properties of the strip in comparison to bulk.

Symbol	Melt temp. [^{0}C]	Rim material	Rollers velocity [m·s^{-1}]	Ejection pressure [MPa]	Pre-set gap [μm]	Nozzle hole [mm]	Thickness [μm]	Width [mm]
T1395	1395	Cu-Be-Co	0.6	0.025	100	3.0	296	45
T1400	1400	Cu-Be-Co	0.6	0.025	100	3.0	306	45
T1430	1430	Cu-Be-Co	0.6	0.025	100	3.0	304	45
T1450	1450	Cu-Be-Co	0.6	0.025	100	3.0	305	45

Table 3. Processing parameters and dimension of the strips

Four strips were produced from a previously cast ingots, with a nominal composition of Ni 25 at.%, Ti 50 at% and Cu 25 at.%. In order to get good quality strips processing parameters such a rolls velocity, a pre-set gap, an ejection pressure and diameter of nozzle hole were optimized and remained the same for all castings (Table 3). Casting parameters differs in solidification temperature, in the range 1395 - 1450^{0}C. Obtained strips were about 40 cm long and revealed smooth surface without any visible cracks and inclusions.

In twin roll technique ingot is placed to the quartz crucible fixed directly over a gap between two rolls. After induction melting, the melt is vertically ejected with argon pressure between two rolls rotated in opposite directions. Thin metal layers solidify on the surface of the rolls simultaneously, when the remaining liquid is spread from central part of the gap to its outer side forming the strip (Goryczka, at all 2005). As the crystallization front proceeds from both rolls the columnar grains are developed. Due to the two-sides solidification an interface between solidified shells is formed (Fig. 17).

However, final microstructure depends on the cooling rate, which is realized by combination between solidification temperature and roll velocity, as well as a gap between rotating rolls. In case of a narrow distance between rolls the strip solidifies over the end-point and is subjected to hot rolling. If the distance is wider the end-point is placed below roll's centre interface consist of pores and discontinuities (Goryczka at all, 2005). The microstructure of surface observed in the strip T1395, is shown in Figure 18a. General, in the strip T1395 solidification on wheel surface causes mountain-like ranges continuously strength along the strip. Each range consists of two zones. First one (A), containing fine

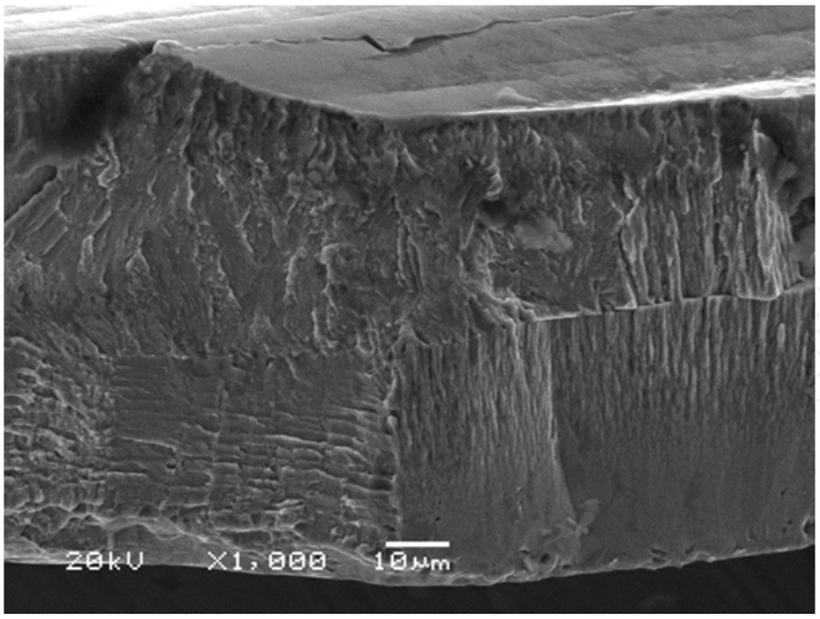

Figure 17. SEM image of fracture in the strip T1395

grains, is associated with hot rolling. Zone B reveals columnar grains growing perpendicular to the hot-rolling direction. Also, the highest applied cooling rate, realized in the strip T1450, causes formation of ranges, however, they consist of separated islands (Fig. 18b). Each island shows presence of zone A and B.

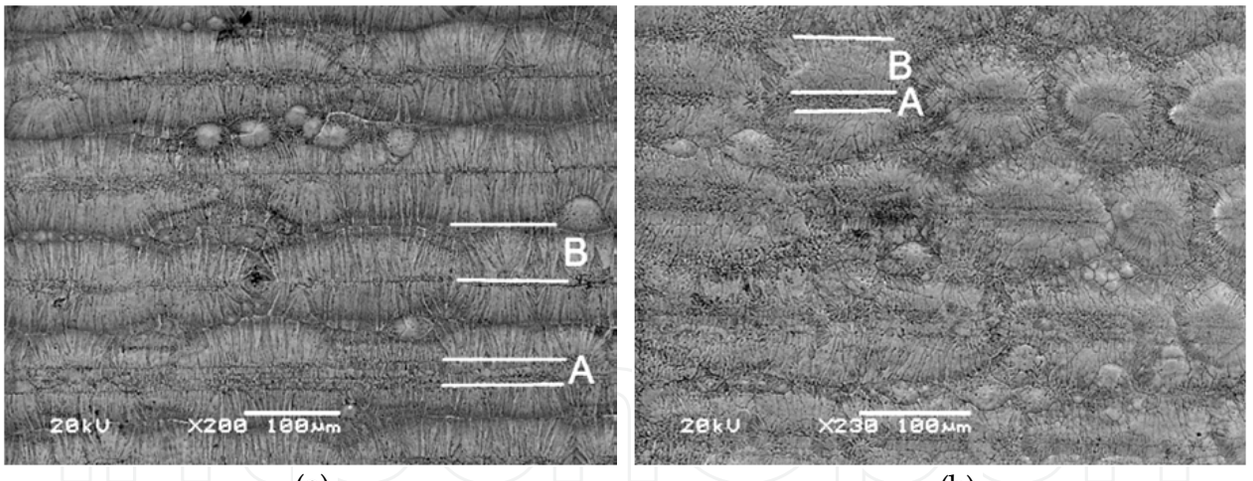

(a) (b)

Figure 18. Surface of the strip T1395 (a) and T1450 (b)

Influence of the solidification temperature on the course of the martensitic transformation was studied using DSC. Figure 19a shows comparison of the DSC cooling/heating curves measured for the as-cast strips. All DSC curves reveal only one exo- and one endothermal peak on cooling and heating, respectively. Similarly, to the sintered blends and melt-spun ribbons, the martensitic transformation occurs in one step. The parent phase transforms to the B19 orthorhombic martensite. From the DSC measurement the transformation temperatures were determined and compared in Figure 19b.

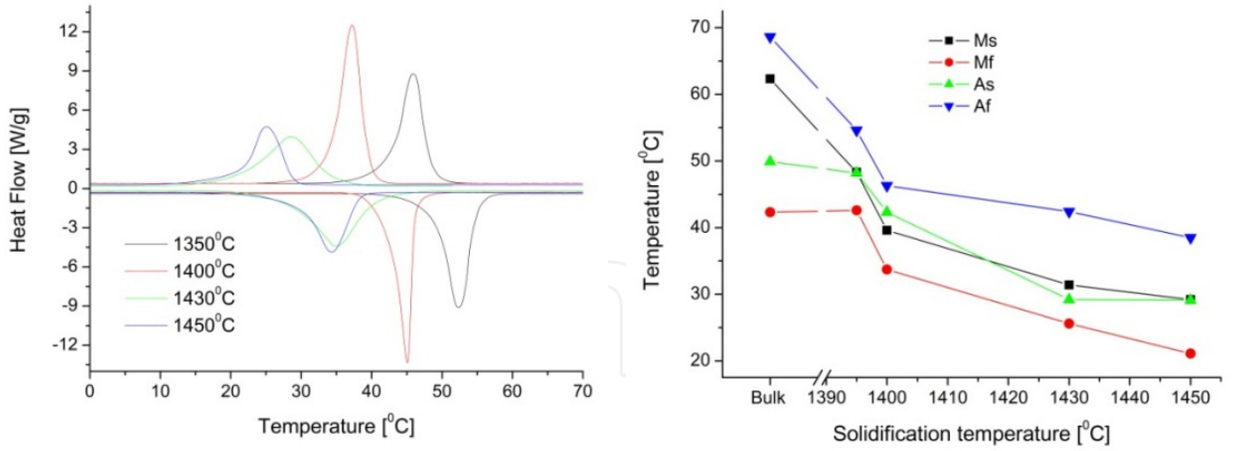

(a) (b)

Figure 19. Comparison of the DSC cooling/heating curves (a) and transformation parameters (b) for as-cast strips.

It can be clearly seen, that increase of solidification temperature affects the transformation temperatures. According to a general trend, the martensitic transformation temperatures represented by M_s, M_f, A_s and A_f are lower in the strips than in the bulk alloys. Especially, this effect is enhanced in the melt-spun ribbons, where cooling rate is several times higher than in the strip. A progressive decrease of reversible and forward martensitic transformation temperature with respect to the bulk alloys was observed. For example, decrease of the A_f temperature reached almost 15 degrees when compare to the results obtained for T1395 and T1450. This is a typical behavior of the as-quenched alloy. Decrease of martensitic transformation temperature is caused by increasing numbers of quenched-in vacancies and stress field surrounded precipitates. Figure 20 shows TEM images of precipitates which were observed in the strips T1395 and T1430. EDS analysis revealed that chemical formula of precipitates is $Ti_2(Ni,Cu)$, which is non-transformable phase – stated in the sintered blends.

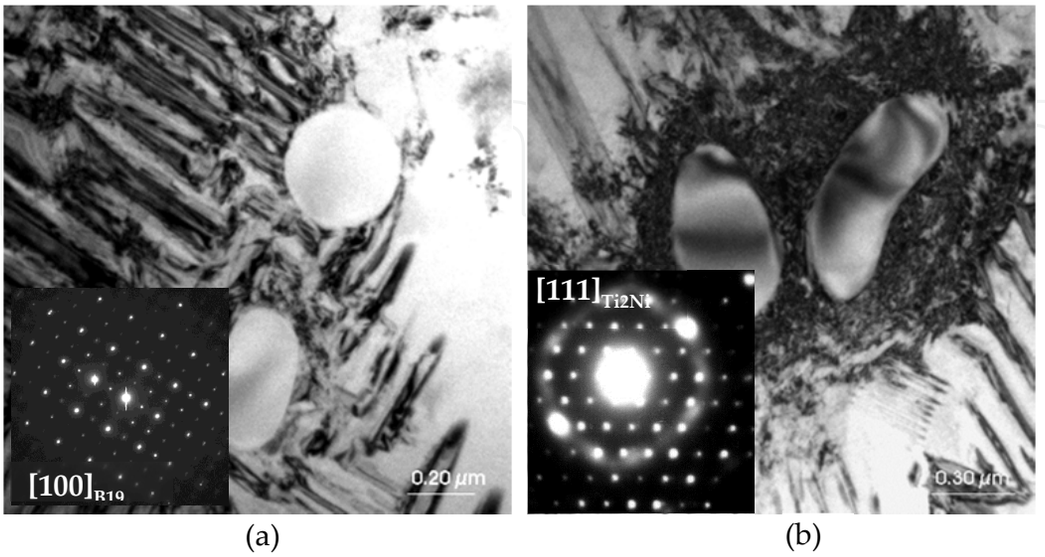

(a) (b)

Figure 20. TEM images of precipitates observed in the strips T1395 (a) and T1430 (b)

Phase identification carried out using electron diffraction pattern proved the Ti_2Ni type of structure for the $Ti_2(Ni,Cu)$ phase (Fig. 20b). Moreover, in the strip produced with higher solidification rate precipitates are surrounded by highly deformed zone (Fig. 20b). It affects the course of the martensitic transformation. In order to trigger martensitic transformation some critical energy is required for nucleation. Energy accommodated around vacancies, dislocation and precipitates decreases driving force of the martensitic transformation. The stress generated in these zones requires additional energy for triggering the start of the martensitic transformation. In consequence, further overcooling is required for transformation continuing. In results of that, the transformation temperatures are moved to the lower thermal region (Fig. 19b). Also, the range of the martensitic transformation and the thermal hysteresis increase (Fig. 21). Additional measure of increasing amount of structural defects and non-transformable phase is degradation of transformation enthalpy. Figure 21 (magenta line) shows enthalpy dependence on solidification temperature. Enthalpy determined for forward and reversible transformation reveal similar behavior – increase of the solidification temperature causes decrease of their value.

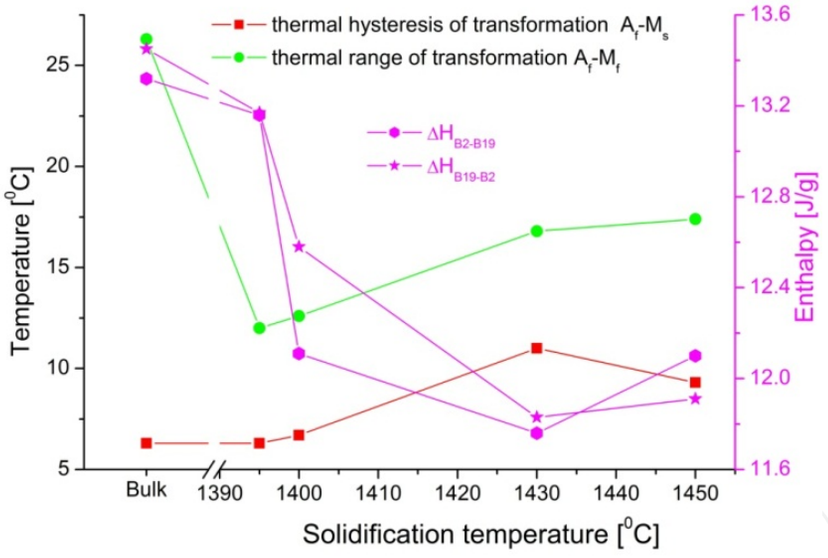

Figure 21. Thermal ranges of the reversible martensitic transformation versus the solidification temperature

4. Summary

This chapter extends the state of knowledge about the technological possibilities of the $Ti_{50}Ni_{25}Cu_{25}$ shape memory alloy manufacturing. It has been proved that, at the stage of alloy production, it is possible to control the reversibility, thermal range and thermal region of the martensitic transformation. Thus, it allows influencing the thermal range of the shape memory effect. Such methods for the $Ti_{50}Ni_{25}Cu_{25}$ alloy manufacture are powders metallurgy, melt-spinning and twin roll casting.

The porous $Ti_{50}Ni_{25}Cu_{25}$ shape memory alloys have been successfully manufactured by powder technology. However, only a correct combination of sintering temperature and time leads to a homogeneous alloy. The best sintering condition for the $Ti_{50}Ni_{25}Cu_{25}$ alloy demands sintering temperature of 1100^0C with the sintering time of 7 hours. Additional thermal treatment such as quenching and additional annealing extends possibility for thermal control of the martensitic transformation. Produced alloy reveals a similar reversible martensitic transformation when compared to dense material. The porosity in homogenous samples does not exceed 25%.

Rapid solidification techniques, realized by means of melt-spinning as well as twin roll casting technique, allows producing fully transformable $Ti_{50}Ni_{25}Cu_{25}$ alloy. The advantage of these techniques, in comparison to traditional casting, is wide possibility for controlling thermal region of the martensitic transformation. Moreover, thin ribbons or strips can be produced directly from the melt in thickness varied from 30 μm to 350 μm. It allows avoiding of mechanical treatment needed after traditionally cast alloy. Also, control of the cooling rate allows for steering of the course of the martensitic transformation.

In melt-spinning technique, the martensitic transformation is sensitive to the wheel speed – processing parameter. Applying speed from the range of 11 m/s -19m/s enables receiving $Ti_{50}Ni_{25}Cu_{25}$ alloy, which transforms in the thermal range from 25^oC to 80^oC. Increase of the cooling rate, realized when melt temperatures is higher than 1350 ^{o}C and the wheel speed increases to 23 m/s, leads to obtaining alloy in amorphous state. However, it opens way for production of nanocrystalline $Ti_{50}Ni_{25}Cu_{25}$ shape memory alloy (Ye Xu, 2009).

Application of the twin roll casting technique moves the thermal range of the martensitic transformation to region between temperatures: 20^oC and 55^oC.

Author details

Tomasz Goryczka
University of Silesia, Institute of Materials Science, Katowice, Poland

Acknowledgement

The author thanks Dr. Patrick Ochin (*ICMPE Institut de Chimie et des Matériaux Paris Est)* for cooperation in shape memory alloys manufacturing with use of rapid solidification techniques.

5. References

B. Yuan X.P. Zhang, C.Y. Chung, M. Zhu *Materials Science and Engineering* A 438–440. - (2006). pp. 585–588.

Berg B.S. *Journal of Materials Processing Technology* 53. (1995). pp. 65-74.

Besseghini S. Villa E., Tuissi A. *Materials Science and Engineering* A273–275. (1999). pp. 390–394.

Ch. Grossmann J. Frenzel, V. Samphath, T. Depka, G. Eggeler, *Metall. Mater. Trans*. 40A. - (2009). - pp. 2531–2544.

F. Dalle G. Despert, Ph. Vermaut, R. Portier, A. Dezellus, P. Plaindoux, P Ochin, *Mater. Sci. Eng.* A 346. - (2003). - pp. 320–327.

F. Fukuda T. Kakeshita, M. Kitayama, K. Saburi, *J. Phys.* IV 5. - (1995). - pp. C8–717.

F.J. Gil E. Solano, J. Penal, E. Engel, A. Mendoza, J.A. Planell, *J. Mater. Sci. Mater. Med.* 15 - (2004). - pp. 1181–1185.

G.E. Monastyrsky V. Odnosum, J. Van Humbeeck, V.I. Kolomytsev, Yu.N. Koval, *Intermetallics* 10 - (2002). - pp. 95–103.

Goryczka T. and Ochin P. *Journal of Materials Processing Technology* 162–163. - (2005). - pp. 178–183.

Goryczka T. Van Humbeeck *J Journal of Alloys and Compunds* 456. - (2008). - pp. 194-200.

Gupta K.P. [Article] // Journal of Phase Equilibria Vol. 23. - 2002. - pp. 541-547.

H. Funakubo *Shape memory alloys*, Amsterdam: Gordon and Breach Science Publisher, 1987.

H. Morawiec T. Goryczka, J. Lelatko, D. Stróż, M. Gigla, P. Tkacz, *Arch. Mater. Sci.* 24. - (2003). - p. 5-21.

H. Rosner P. Schloßmacher, A.V. Shelyakov, A.M. Glezer, *Acta Mater*. 49. - (2001). - p. 1541.

Haga T. Suzuki S. *Journal of Materials Processing Technology* 118. - (2001). - pp. 165-168.

Haga T. Takahashi K., Ikawa M., Watari H *Journal of Materials Processing Technology* 140. - (2003). - pp. 610-615.

Van Humbeeck J. *J. Phys. IV France* 7. - (1997). - pp. C5-3-C5-11.

Itala AI Ylanen HO, Ekholm C, Karlsson KH, Aro HT. *J Biomed Mater Res.* 58. - (2001). - pp. 679-683.

J. Morgiel E. Cesari, J. Pons, A. Pasko, J. Dutkiewicz, *J. Mater. Sci.* 37. - (2002). - pp. 5319–5325.

J.E. Hanlon S.R. Butler and R.J. Wasilewski, *Trans. AIME 239*. - (1967). - pp. 1323-1327.

Karageorgiou V Kaplan D. *Biomaterials* 26. - 2005. - pp. 5474-5491.

Kima H.Y. Kima J.I., Inamura T., Hosoda H., Miyazaki S. *Mat. Sci.e and Eng. A* 438–440. - (2006). - pp. 839–843.

Li B.Y., Rong, L.J., Li, Y.Y., Gjunter, V.E., *Intermetallics* 8. - 2000. - pp. 881–884.

Li C. Zheng Y. F. *Materials Letters* 60 - (2006). - pp. 1646–1650..

Melton: O. Mercier and K. N *Met. Trans. A,*. - (1979). - Vol. 10A. - p. 387.

Mercier: K. N. Melton and O. *Met. Trans. A,*. - (1978). - Vol. 9A. - p. 1487.

Morawiec H. Stróż D., Goryczka T., Chrobak D. *Scripta Materialia* 35. - (1996). - pp. 485-490.

Nomura K. Tsuji and K. *J. Mater. Sci.,* 27,. - 1992. - p. 2199.

Nomura K. Tsuji and K. *Scripta Metall.,* 24. - 1990. - p. 2037.

Otsuka K. Wayman C. M. *Shape Memory Materials* Cambridge: Cambridge University Press, (1998).

R. Santamarta E. Cesari, J. Pons, T. Goryczka, *Metall. Mater. Trans.* 35A. - (2004). - pp. 761–770.

S. Colombo C. Cannizzo, F. Gariboldi, G. Airoldi, *J. Alloys Compd.* 422. - (2006). - pp. 313–320.

S. Eucken J. Hirsch *Mater. Sci. For.* 56–58. - (1990). - p. 487.

Santamarta R. Segui C., Pons J., Cesari E. *Scripta Materialia* 41. - (1999). - pp. 867–872.

Simske SI and Sachdeva R. *J Biomed Mater Res.* 29. - (1995). - pp. 527-533.

T. Goryczka, M. Karolus, H. Morawiec, P. Ochin *Journal de Physique IV*, 11. - (2001). - pp. Pr8-345.

T. Goryczka P. Ochin, H. Morawiec *Archives of Metallurgy and Materials,* 49. - (2004). - pp. 891-906.

T.H. Nam T. Saburi and K. Shimizu, *Mater. Trans. JIM.*, 31. - 1990. - p. 959.

T.W. Duerig K.N. Melton, D. Stockel, C.M. Wayman *Engineering aspects of sahpe memory alloys* - London: Butterworth-Heinemann, 1990.

W. J. Moberly and K.N. Melton at *"Engineering aspects of shape memory alloys"* by T.W. Duering K.N Melton, D. Stöckel, C.M. Wayman, Butterworth-Heinemann Ltd. 1990, p.52.

W.M. Stoobs J.V. Wood *Acta Met.* 27. - (1979). - p. 575..

Ye Xu Xu Huang, A.G. Ramirez *Journal of Alloys and Compounds* 480. - (2009). - pp. L13–L16.